Optimizing Hydrological Pan Evaporation Prediction Using Advanced Machine Learning Techniques with Spectral Clustering

Labib Sharrar

AUIQ TECHNICAL ENGINEERING SCIENCE 2025;2:83–99

ORIGINAL STUDY

Optimizing Hydrological Pan Evaporation Prediction Using Advanced Machine Learning Techniques with Spectral Clustering

Labib Sharrar

Electrical, Computer and Energy Engineering Department, Faculty of Engineering, University of Colorado, Boulder, CO, 80309, USA

ABSTRACT

Accurate prediction of pan evaporation remains a significant challenge due to inconsistencies across different climatic regions. This study aims to enhance pan evaporation estimation by developing a robust hybrid machine learning (ML) model that integrates spectral clustering with advanced regression techniques, specifically the Histogram-based Gradient Boosting Regressor (HGBR) and Extreme Gradient Boosting Regressor (XGBR), to improve prediction accuracy and adaptability across diverse environments. The research developed a novel methodology by employing spectral clustering for models' performance enhancement, followed by rigorous hyperparameter tuning, sensitivity analysis to assess the impact of individual features on each model. Finally, models underwent lack of fit test to confirm model adequacy and usability. The findings of the study revealed that the HGBR model outperformed the XGBR, this is evidenced by its consistent training and testing results (training R^2 of 0.94 and RMSE of 1.34; testing R^2 of 0.92 and RMSE of 1.45) both training and testing observed close enough for judging on the robustness of the model compared to the XGBR (training R^2 of 0.96 and RMSE of 1.11; testing R^2 of 0.91 and RMSE of 1.48) which raises the issue of overfitting due to large gap between the R2 values for training and testing. These results demonstrate the HGBR model's superior robustness and reliability for predicting pan evaporation. The research contributes significantly to local and global water resource management strategies by providing a reliable predictive tool and sets a foundation for future studies to further refine these models and explore their applicability in other geographical settings.

Keywords: Hydrological forecasting, Climate adaptation technologies, Predictive water resource modeling, Advanced regression analysis, Water cycle management, Environmental machine learning

1. Introduction

Pan evaporation is a vital hydrological variable that directly impacts water resource management, agricultural planning, and climate studies [1–3]. It refers to the rate at which water evaporates from a standardized open pan, serving as a crucial indicator for estimating evaporation rates of larger water bodies and assisting in the management of water supplies, especially in agricultural and arid regions [4–6]. Accurate estimation and prediction of pan evaporation are essential for developing effective water management strategies, optimizing irrigation practices, and enhancing our understanding of climate dynamics [7, 8]. These predictions help in foreseeing water shortages, planning for drought conditions, and ensuring sustainable water utilization, which is particularly critical in regions facing irregular rainfall patterns and increasing water demand due to population growth and industrialization [9, 10]. As climate change continues to alter hydrological cycles globally, the ability to predict changes in evaporation rates becomes increasingly important for adapting to these impacts and mitigating potential water-related conflicts [11, 12]. To set the stage for this investigation, recent

Received 11 February 2025; revised 9 April 2025; accepted 13 April 2025.
Available online 30 April 2025

E-mail address: Labib.Sharrar@colorado.edu (L. Sharrar).

https://doi.org/10.70645/3078-3437.1026

advancements in ML applications for pan evaporation prediction across diverse regions are examined.

Traditional pan evaporation estimation methods often rely on empirical formulas such as Hargreaves or Blaney–Criddle [13]. While these methods are computationally simple, they are typically tailored to specific climates and rely on a limited number of inputs, which limits their generalizability [14]. In contrast, machine learning models can adapt to complex, nonlinear interactions among multiple meteorological variables, offering improved accuracy and robustness across diverse climatic regions [15]. This adaptability is particularly valuable in the face of climate change, where dynamic environmental conditions demand more flexible and data-driven modeling approaches. Similar efforts have demonstrated the value of statistical modeling for hydrological applications [16].

Recent studies have utilized various ML approaches to enhance the prediction accuracy of pan evaporation across different geographical settings. For instance, a study in the Yangtze River Basin, China, utilized a Fuzzy Genetic (FG) algorithm along with other models to estimate monthly pan evaporation, demonstrating the model's effectiveness in generalizing across multiple locations with diverse climatic inputs [17]. Similarly, in Queensland, Australia, a hybrid Long Short-Term Memory (LSTM) model integrated with Neighborhood Component Analysis significantly outperformed traditional models by incorporating feature selection alongside deep learning techniques to enhance daily pan evaporation predictions [18]. In contrast, research conducted in the Indian Central Himalayas explored the efficacy of multiple ML models, where the Multi-gene Genetic Programming (MGGP) and Multiple model-artificial neural network (MM-ANN) showed high effectiveness during testing periods [19]. For a detailed overview of additional studies, refer to Table 1. These variations in model performance across studies raise the question of how the integration of advanced ML techniques, such as spectral clustering, can further improve the accuracy and reliability of pan evaporation predictions across different environments. This research aims to address this gap by developing and validating an advanced hybrid ML model tailored to optimize pan evaporation forecasting in diverse climatic conditions.

Despite significant advancements in pan evaporation modeling, existing predictive models often struggle with adaptability across varying climatic conditions and lack robustness in diverse geographic settings. Unlike previous studies that apply machine learning (ML) models directly, this research introduced a novel hybrid approach that integrates spectral clustering as a performance-enhancing preprocessing step prior to model training. This method improves data homogeneity, allowing the subsequent ML models Histogram-based Gradient Boosting Regressor (HGBR) and Extreme Gradient Boosting Regressor (XGBR) to learn more effectively from the underlying patterns. By addressing key limitations in generalization and interpretability, the proposed framework offers a more adaptable and reliable solution for pan evaporation prediction. Locally, it provides precise tools for managing water resources in regions with fluctuating climates, directly benefiting agricultural planning and drought mitigation strategies. Globally, it enhances the understanding of hydrological cycles impacted by climate change, equipping policymakers and stakeholders with robust forecasting tools. Overall, this study bridges critical gaps in current modeling practices and sets a foundation for future research that integrates advanced computational techniques into environmental and hydrological sciences. The primary objective of this research is to develop and validate an advanced hybrid ML model that incorporates spectral clustering with Hyperparameter-Tuned Histogram-based Gradient Boosting Regressor (HGBR) and Extreme Gradient Boosting Regressor (XGBR) to predict pan evaporation accurately. This model aims to achieve superior performance metrics compared to existing models by: (i) Enhancing the understanding of the relationship between climatic variables and evaporation rates. (ii) Providing a robust prediction tool that can be adapted to various geographical locations and climatic conditions. (iii) Contributing to the global efforts in water resource management by offering a reliable model for predicting water availability and potential drought conditions. By fulfilling these objectives, this study will not only contribute to the scientific community by advancing the methodologies used in hydrological modeling but also aid policymakers and stakeholders in making informed decisions regarding water management and agricultural practices.

2. Methods and materials

2.1. Models' development

In the development of our predictive models, the process begins with data collection and analysis, which is immediately followed by data pre-processing to ensure quality and consistency. This processed data is then split into two parts, where 70% were allocated for training and 30% for testing models' performances, ensuring that model evaluation reflects an unbiased estimation of performance. The primary models developed include the (XGBR and HGBR), where hyperparameter tuning is conducted to optimize performance. After training, the models undergo a validation phase where their

Table 1. Comprehensive review of existing studies on the analysis of ML Approaches for pan evaporation modeling across different geographic locations and time periods.

Reference	Geographic Location	Data Period	Model(s) Used	Main Findings	Limitations
[8]	Iraq (Baghdad, Basrah, Mosul)	1990–2013 for Baghdad and Mosul, 1990–2012 for Basrah	Conditional Random Forest Regression (Cforest), Multivariate Adaptive Regression Splines (MARS), Bagged Multivariate Adaptive Regression Splines (BaggedMARS), Model Tree M5, K-nearest Neighbor (KNN), Weighted K-nearest Neighbor (KKNN)	The study demonstrated that the Weighted K-nearest Neighbor model provided the best accuracy in modeling monthly pan evaporation across three locations in Iraq.	The models may require adaptation to different climatic conditions or regions to maintain accuracy.
[7]	Chhattisgarh, India	1981–2015	Deep-LSTM, MLANN, Empirical Methods (Hargreaves and Blaney–Criddle)	Deep-LSTM models demonstrated superior accuracy in predicting daily pan evaporation with minimal input features across three distinct agro-climatic zones compared to MLANN and empirical models.	The study suggests further testing in other agro-climatic conditions for generalizability.
[20]	Sidi Mohammed Ben Abdellah reservoir, Morocco	June 2021–June 2022	Deep Neural Network (DNN), Support Vector Regression (SVR), Extra Tree, XGBoost	Developed an interpretable ML framework that accurately predicts daily pan evaporation using hourly climate data. Identified key climate variables using tools like SHAP.	Challenges with “black-box” ML models which lack interpretability and transparency, limiting practical application.
[21]	Poyang Lake Basin, Southern China	2001–2015	Extreme Learning Machine (ELM) coupled with Whale Optimization Algorithm (WOA) and Flower Pollination Algorithm (FPA)	The study introduced hybrid models (FPAELM and WOAELM) that outperformed traditional models in predicting monthly pan evaporation, demonstrating the effectiveness of hybrid approaches.	The study points to the complexity of “black-box” ML models, which may hinder practical applicability without adequate interpretability.
[17]	Yangtze River Basin, China	1961–2000	Fuzzy Genetic (FG) Algorithm, ANFIS-GP, M5 Model Tree	The study highlighted the FG model’s superior performance in estimating monthly pan evaporation using various climatic inputs across multiple stations. It effectively generalized across six different locations.	The complexity of “black-box” ML models may limit practical applicability without adequate interpretability.
[18]	Queensland, Australia (Amberley, Gatton, Oakey, & Townsville)	31 August 2002 to 22 September 2020	Hybrid Long Short-Term Memory (LSTM) model integrated with Neighbourhood Component Analysis (NCA)	The NCA-LSTM hybrid model significantly outperformed benchmark models in predicting daily pan evaporation using a hybrid approach that integrated feature selection with deep learning.	The complexity of “black-box” ML models and the requirement for extensive data preprocessing were noted as limitations.

(Continued)

Table 1. Continued

Reference	Geographic Location	Data Period	Model(s) Used	Main Findings	Limitations
[22]	Fars Province, Iran	2006–2021	Multilayer Perceptron (MLP) with Bayesian Regularization (BR) and Scaled Conjugate Gradient (SCG) algorithms	The MLP-BR model showed the best performance in predicting daily pan evaporation using a combination of temperature, pressure, and humidity inputs, with enhanced performance over traditional MLP trained with the LM algorithm.	The complexity and "black-box" nature of ML models limit their interpretability and practical applicability without thorough validation.
[23]	Kuwait	Not explicitly stated, validation from June 2021 to June 2022	Support Vector Machine (SVM), Gaussian Processes, Regression Trees	Employed SVM, Gaussian Processes, and Regression Trees to model daily pan evaporation successfully in arid climates. Demonstrated robust performance of data-driven models over traditional methods.	Black-box nature of models limits practical application without deeper interpretability. High evaporation rates challenge model accuracy.
[24]	Pusa, Bihar, India	June 2013–September 2017	Artificial Neural Network (ANN), Wavelet-based ANN (WANN), Radial Function-based SVM (SVM-RF), Linear Function-based SVM (SVM-LF), Multi-linear Regression (MLR)	The study demonstrated that the SVM-RF model outperformed other models in all tested scenarios, highlighting the effectiveness of integrating wavelet transformation with SVM for modeling daily pan evaporation.	The complexity of models and the need for extensive data preprocessing were noted as limitations.
[19]	Indian Central Himalayas	Not explicitly stated	Multiple model-artificial neural network (MM-ANN), Multivariate Adaptive Regression Spline (MARS), Support Vector Machine (SVM), Multi-gene Genetic Programming (MGGP), and M5Tree	The study assessed several AI models for simulating monthly pan evaporation using climatological data. MM-ANN and MGGP were found to be the most effective during testing periods.	The complexity of "black-box" ML models may limit practical applicability without adequate interpretability.

accuracy is assessed. Once accuracy criteria of models were satisfied the models went under a sensitivity analysis, where, exposing impactful and non-impactful features on the output. Subsequently models undergone a Lack of Fit Test to determine their usability. In case a model indicates significant with pure error, the model is marked as unusable. Conversely, models that pass the lack of fit test (not significant with respect to pure error), marked as final usable model, after which the final model is saved, marking the end of the process (Fig. 1).

2.2. Data collection and analysis

The dataset used in this study was obtained from a published paper [25], where it indicated the process of dataset collection as follows: the data collected in the form of observational from the extensive meteorological records maintained by the Kermanshah Regional Water Authority. These records comprise a comprehensive dataset spanning a 30-year period from (1988 to 2018), collected at the Kermanshah synoptic station located in Iran (Fig. 2). This region, known for its unique climatic conditions, provides a rich source of environmental data vital for hydrological studies. The data cover monthly measurements of different meteorological variables critical for pan evaporation prediction, including maximum and minimum temperatures, maximum and minimum relative humidities, sunshine hours, rainfall, wind speed, and the evaporation. The collection of such diverse data types over an extended period allows for a robust analysis of the factors influencing evaporation, which is vital for improving water resource management in

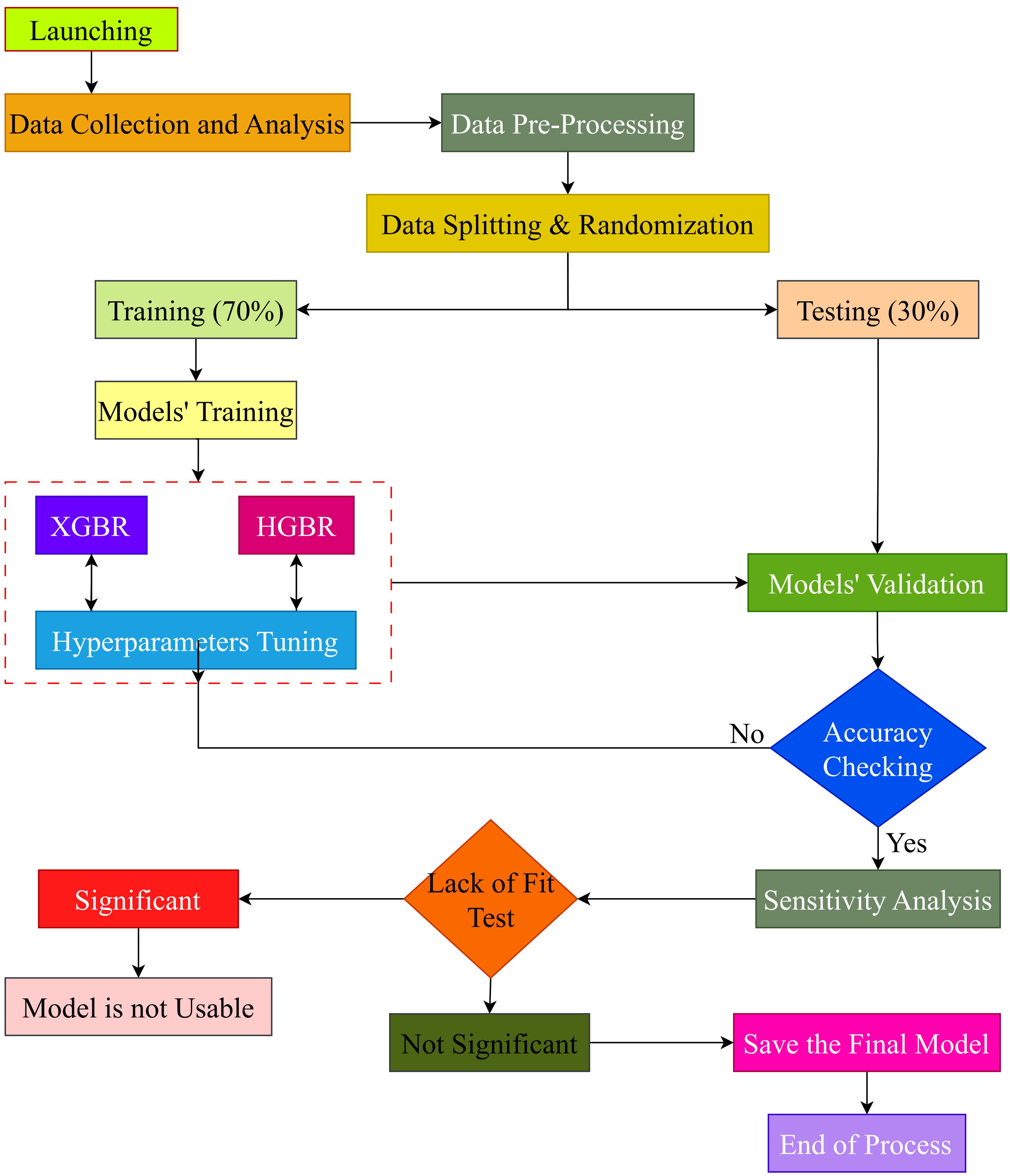

Fig. 1. Models development flowchart.

arid and semi-arid regions. It should be noted that data for the climatic variables are collected using Earth observational monitoring stations.

As outlined in Table 2, the dataset consists of 372 entries for each variable, providing a substantial sample size for analysis. The descriptive statistics, including the mean, standard deviation, minimum, median, and maximum values, alongside measures of skewness and kurtosis, offer insights into the distribution and variability of each meteorological factor. For instance, the maximum temperature exhibits a mean of 23.64°C and varies from 0.27°C to 40.15°C, with a

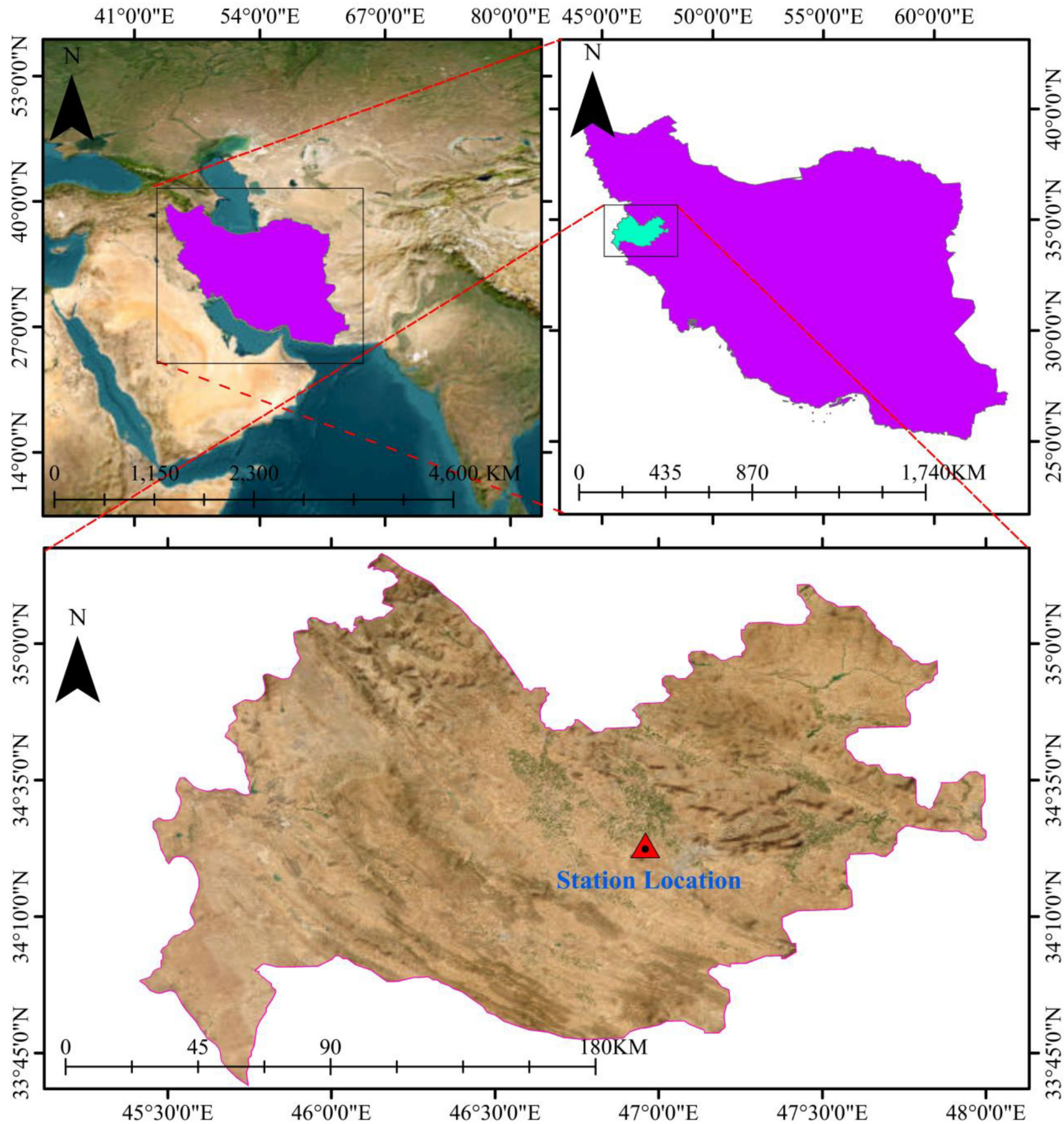

Fig. 2. Study region map, (a) Iran map located on world map, (b) Iran map, and (c) Study region map with station located on.

slightly left-skewed distribution (skewness = −0.02) indicating a bulk of data points amassed towards the higher end of the temperature range. In contrast, rainfall demonstrates a high degree of variability (standard deviation = 33.95 mm) and a pronounced right skew (skewness = 1.37), reflecting that most of the data points are near zero with occasional high values, which is typical for precipitation data. Moreover, frequency visualizations of the data revealed the distribution patterns of each variable (Fig. 3). Maximum and minimum temperatures showed a balanced distribution, typical of the region's thermal characteristics. Relative humidity, both maximum and minimum, exhibits a skewed distribution towards higher values, indicating occasional high humidity in generally dry conditions. Sunshine hours are predominantly high, aligning with the area's sunny climate. Rainfall data are right-skewed, reflecting infrequent but sometimes

Table 2. Statistics of the data.

Features	data	mean	std	min	25%	50%	75%	max	skew	kurt
Max temperature (°C)	372	23.64	10.78	0.27	14.15	23.67	34.05	40.15	−0.02	−1.31
Min temperature (°C)	372	7.02	7.08	−10.42	1.12	7.07	12.76	20.31	0.04	−1.06
Max relative humidity (%)	372	62.90	23.63	20.00	38.14	71.74	84.28	95.61	−0.32	−1.49
Sunshine (h)	372	7.99	2.51	3.16	5.76	7.53	10.34	12.63	0.10	−1.24
Min relative humidity (%)	372	24.74	13.92	3.20	12.37	24.02	34.42	65.84	0.43	−0.55
Rainfall (mm)	372	28.83	33.95	0.00	0.00	17.95	46.63	162.50	1.37	1.72
Wind speed (m/s)	372	2.49	0.57	0.85	2.13	2.52	2.91	4.04	−0.33	−0.17
Evaporation (mm)	372	6.75	5.25	0.10	2.11	5.61	11.16	21.70	0.60	−0.70

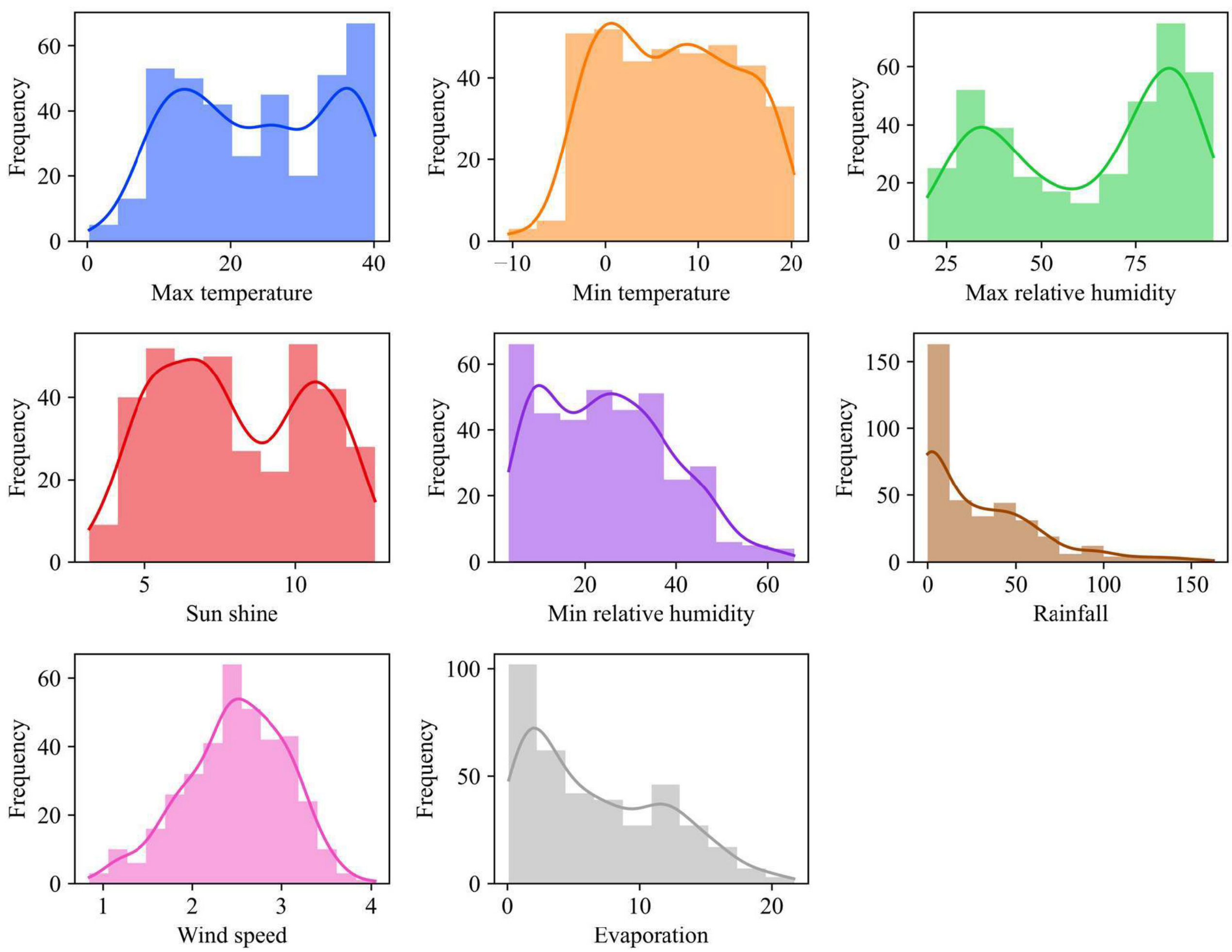

Fig. 3. Frequency visualization of the data.

heavy precipitation. Wind speed follows a normal distribution, suggesting steady wind conditions without extreme variations. This analysis confirms the dataset's consistency and representativeness for modeling evaporation in semi-arid environments. To further delve into the relationships between these variables and their influence on the output (evaporation), a correlation coefficient (CC) heatmap was developed, as shown in Fig. 4. This heatmap provides a clear visual representation of how each variable interrelates with others, with strong correlations visible between, for example, evaporation and both maximum and minimum temperatures 0.92 and 0.91 respectively, suggesting that higher temperatures significantly enhance evaporation rates.

2.3. Data-preprocessing

In the data preprocessing phase, the dataset underwent a thorough evaluation for missing values and outliers to ensure robust model performance.

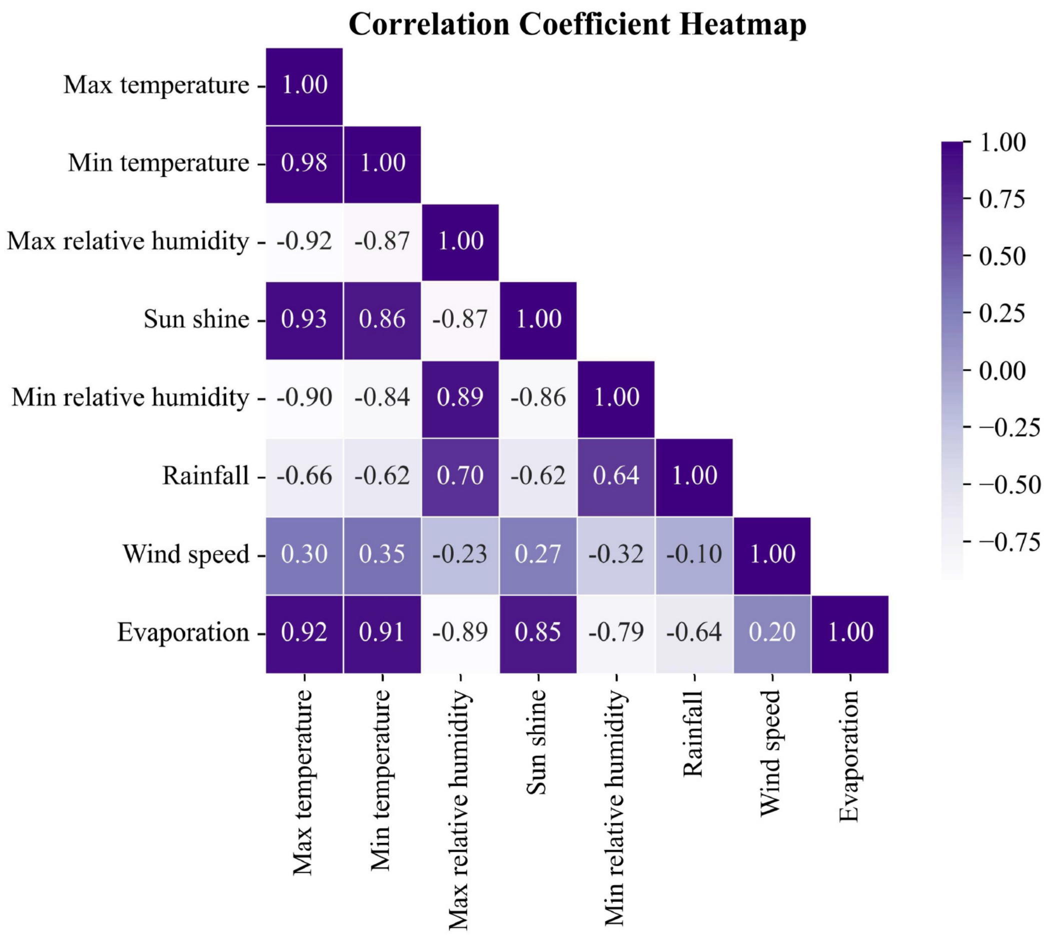

Fig. 4. Correlation coefficient's heatmap of inputs vs output.

Given that this dataset was previously utilized in another study, it was confirmed to contain no missing values, and all records were validated as accurate observations. Attempts to transform the features to enhance correlations between inputs and output did not yield significant improvements. Therefore, the original features were retained without modification for subsequent analysis. This approach ensured the integrity and reliability of the data used in developing our predictive models. Broader hydrological modeling studies have also emphasized the role of input data characteristics in shaping model reliability [26].

2.4. Spectral clustering

To enhance the performance of our predictive models, we implemented spectral clustering as a pivotal preprocessing step. Spectral clustering is a technique that utilizes the eigenvalues of a similarity matrix derived from the data to perform dimensionality reduction before clustering [27–29]. This method effectively captures complex structures within the data by identifying groups of similar data points based on their relationships, rather than their absolute distances from each other [30, 31]. By applying spectral clustering, we aimed to improve the homogeneity within each cluster, which in turn facilitates more accurate and robust modeling. This approach is especially beneficial for handling multi-dimensional data where traditional clustering techniques may falter, thus potentially leading to enhanced model performance.

2.5. Utilization of machine learning models

In this study, advanced ML models used to predict hydrological evaporation more accurately by making use of complex nonlinear relationships within the data. ML offers a dynamic approach to model development that adapts to the intricacies of environmental data, vitally enhancing predictive accuracy over traditional statistical methods. The models chosen for this study, specifically the HGBR and XGBR, were selected due to their robustness in handling varied datasets and their capability to improve prediction performance through iterative learning and fine-tuning of decision trees. These models are described in detail in the following sections, outlining their specific contributions to the study's objectives.

2.5.1. HGBR model

The HGBR is a powerful ensemble ML technique that builds upon decision trees using a gradient boosting framework. It constructs a model in a stage-wise fashion and generalizes them by allowing optimization of arbitrary differentiable loss functions. In each stage, a regression tree $h(x)$ is fit on the negative gradient of the loss function L, which is used to predict the residuals or errors [32–34]. The formula for updating the model is:

$$L\left(y, F(x)\right) = \sum_{i=1}^{n} (y_i - F(x_i))^2 \tag{1}$$

where y_i are the actual values, and $F(x_i)$ are the predicted values. The model iteratively improves predictions over M boosting stages, with each stage attempting to correct the errors of the previous stages using the formula:

$$F_m(x) = F_{m-1}(x) + \gamma h(x) \tag{2}$$

where $F_{m-1}(x)$ is the model from the previous iteration, $h(x)$ is the current regression tree, and γ is the learning rate [32]. This method is particularly effective for handling large datasets and provides an improved accuracy by focusing learning on hard cases that previous iterations found challenging to predict.

2.5.2. XGBR model

The XGBR employs a sophisticated ensemble technique that employs gradient boosting algorithms tailored for speed and performance [35, 36]. XGBR optimizes both computational efficiency and model performance by constructing new models that learn to correct the errors made by earlier models in the ensemble [37, 38]. The formula for the model is:

$$F_m(x) = F_{m-1}(x) + \eta \cdot h(x) \tag{3}$$

where $F_{m-1}(x)$ indicates the model obtained from the previous iteration, $h(x)$ is the new regression tree, and η is the learning rate, controlling the contribution of each tree to the final model. Model's efficiency in handling various types of data, including non-linear and complex patterns, makes it an excellent choice for enhancing the predictive accuracy in our study.

2.6. Models' performance evaluation metrics

To assess the effectiveness of the developed models, several statistical metrics were used that capture different aspects of model performance. These metrics provide a comprehensive evaluation of the models' accuracy and reliability:

(i) Coefficient of Determination (R^2): Measures the proportion of variance in the dependent variable that is predictable from the independent variables. It is a key indicator of model fit quality [39–41].

$$R^2 = 1 - \frac{\sum_{i=1}^{n} \left(y_i - \hat{y}_i\right)^2}{\sum_{i=1}^{n} \left(y_i - \bar{y}\right)^2} \tag{4}$$

(ii) Root Mean Square Error (RMSE): Provides a measure of the differences between values predicted by a model and the values observed. It is especially useful for comparing prediction errors across different datasets or models [39, 40, 42].

$$RMSE = \sqrt{\frac{1}{n} \sum_{i=1}^{n} \left(y_i - \hat{y}_i\right)^2} \tag{5}$$

(iii) Mean Absolute Error (MAE): Represents the average absolute difference between the observed actual outcomes and the predictions made by the model. It offers a straightforward interpretation of overall prediction error [39, 42].

$$MAE = \frac{1}{n} \sum_{i=1}^{n} |y_i - \hat{y}_i| \tag{6}$$

(iv) Median Absolute Error (MedAE): This metric provides the median of all absolute differences between the target values and the predictions made by the model. It is robust to outliers and useful in skewed datasets [39, 43].

$$MedAE = \text{median}\left(|y_1 - \hat{y}_1|, |y_2 - \hat{y}_2|, \ldots, |y_n - \hat{y}_n|\right) \tag{7}$$

In the above metrics equations, $\hat{y}_i$ indicates predicted values, where y_i is observed value and n providing the number of observations. These metrics were selected for their individual ability to provide detailed insights into all aspects of the model's performance, ensuring a balanced assessment. They allow us to identify models that not only perform well on average but also maintain accuracy across a range of possible values.

3. Results representation

3.1. Comparative analysis of HGBR and XGBR model's performance

In evaluating of the performance of the HGBR and XGBR models for pan evaporation prediction, key metrics such as R^2, RMSE, MAE, and MedAE were employed for both the training and testing phases. The HGBR model showed a robust performance with an R^2 of 0.94, RMSE of 1.34, MAE of 0.97, and MedAE of 0.75 in the training phase, and demonstrated consistency in the testing phase with an R^2 of 0.92, RMSE of 1.45, MAE of 1.11, and MedAE of 0.87. The XGBR model, while showing slightly higher accuracy in the training phase with an R^2 of 0.96, RMSE of 1.11, MAE of 0.83, and MedAE of 0.63, exhibited more significant decreases in the testing phase to an R^2 of 0.91, RMSE of 1.48, MAE of 1.13, and MedAE of 0.85 (Fig. 5). The smaller gap in performance metrics between the training and testing phases for the HGBR model suggests it is more consistent model and less prone to overfitting compared to the XGBR, which displayed a more considerable performance drop-off between the two phases. Thus, the HGBR model outperformed the XGBR model, indicating a more reliable and stable prediction capability for the pan evaporation in this research.

Beyond the primary statistical metrics, a closer inspection of the scatter plots further reinforced the comparative reliability of the HGBR model. The HGBR's predictions align more closely along the 1:1 reference line in both training and testing sets. This indicated a better capture of the underlying functional relationship between observed and predicted pan evaporation values. The tight clustering around the diagonal line in the HGBR model panels suggested lower variance and fewer outliers. This is particularly evident in the testing phase. In contrast, although the XGBR model achieved a marginally higher training R^2, the increased dispersion of testing data points away from the diagonal line revealed a model more susceptible to overfitting. This deviation becomes more pronounced for higher evaporation values where XGBR model tends to underpredict. Additionally, the HGBR model's slightly higher MedAE in training but lower increase in testing underscored its ability to maintain robustness without sacrificing generalization. These visual and statistical insights, taken together, provided compelling evidence that the HGBR model offered more balanced and dependable performance under unseen conditions. Which made it a more practical choice for real-world hydrological forecasting applications.

3.2. Comprehensive evaluation of HGBR and XGBR models using bar charts and Taylor diagram

The comparative analysis of HGBR and XGBR models using performance metrics and Taylor diagram. The HGBR model demonstrated a training R^2 of 0.94, RMSE of 1.34, MAE of 0.97, and MedAE of 0.75, with a slight decrease in testing performance to an R^2 of 0.92, RMSE of 1.45, MAE of 1.11, and MedAE of 0.87. Conversely, the XGBR model yielded a higher training R^2 of 0.96 with an RMSE of 1.11, MAE of 0.83, and MedAE of 0.63, though it experiences a drop in testing performance to an R^2 of 0.91, RMSE of 1.48, MAE of 1.13, and MedAE of 0.85. Further, the Taylor diagram clarifies each model's consistency and accuracy in training and testing phases. The HGBR model maintained close correlation coefficients between training CC = 0.97 and testing CC = 0.96 with standard deviations slightly changing from 4.8 to 4.7. The XGBR model, while showing a higher training CC of 0.99, demonstrated a more considerable decrease in testing to CC of 0.94 with a consistent standard deviation of 4.8 across both phases (Fig. 6). These findings reinforce the earlier results, showing HGBR's higher consistency and reduced risk of overfitting compared to XGBR, thereby confirming HGBR model as the more reliable algorithm for predicting the pan evaporation in varied settings.

Further, the integration of bar charts and Taylor diagram offered a holistic perspective on both the magnitude and distributional consistency of model performance across both phases. The bar charts distinctly illustrated that while XGBR model showed slightly better training (e.g., lower RMSE and MAE), the HGBR model maintained a more balanced and stable transition into the testing phase, with minimal deterioration in all four-performance metrics. This behavior indicated that HGBR model generalizes better and avoids the common pitfall of overfitting that is subtly evident in XGBR model's results. More compelling insights emerged from the Taylor diagram, where the proximity of HGBR model's testing phase demonstrated its strong correlation with observed values (CC = 0.96) and minimal deviation in standard deviation (4.7 vs. 4.8 for training). In contrast, although XGBR model exhibited an exceptionally high training correlation (CC = 0.99), the drop to 0.94 in testing, coupled with its fixed standard deviation, suggested a narrower learning range that may struggle with variability in unseen data.

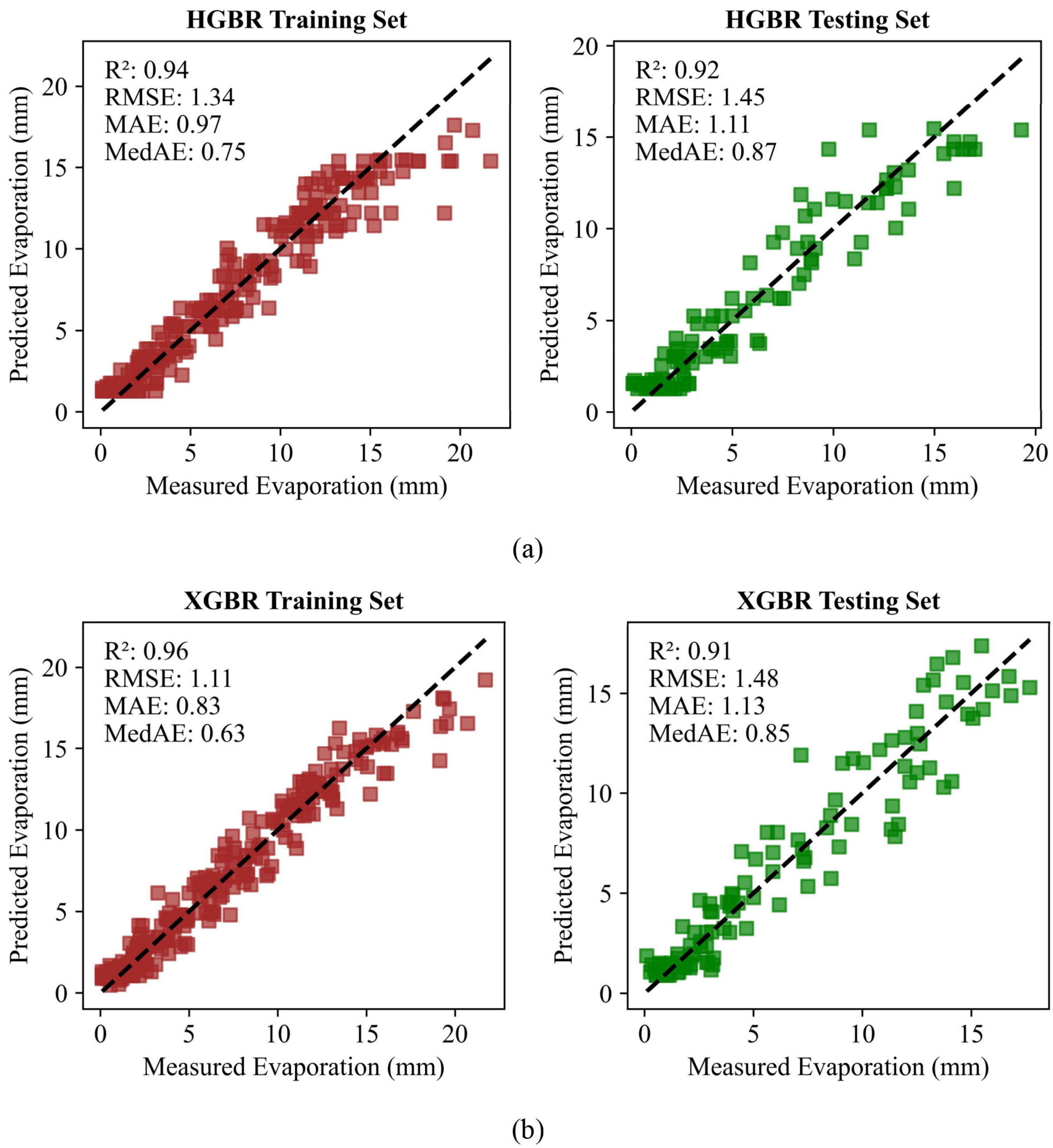

Fig. 5. Performance comparison ML models in predicting pan evaporation: (a) HGBR model training and testing performance; (b) XGBR model training and testing performance.

3.3. Sensitivity analysis

The sensitivity analysis revealed the impact of eliminating various features on the performance of the HGBR and XGBR models. For the HGBR model, eliminating minimum relative humidity proved most impactful, significantly increasing the RMSE in testing to 1.60 from the baseline of 1.45 and decreasing the R^2 to 0.90, indicating a lower model accuracy without this feature (Table 3). In contrast, eliminating sunshine had the least impact, with the model maintaining a testing R^2 of 0.92 and an RMSE of 1.45, nearly identical to the baseline. For the XGBR model, the removal of minimum temperature had the most significant effect, reducing the testing R^2 to 0.90 and increasing the RMSE to 1.56. Eliminating wind speed had the least effect, with the testing R^2 slightly improving to 0.93 and the RMSE decreasing to 1.36, showing robust model performance even without this variable. These results underscore the critical

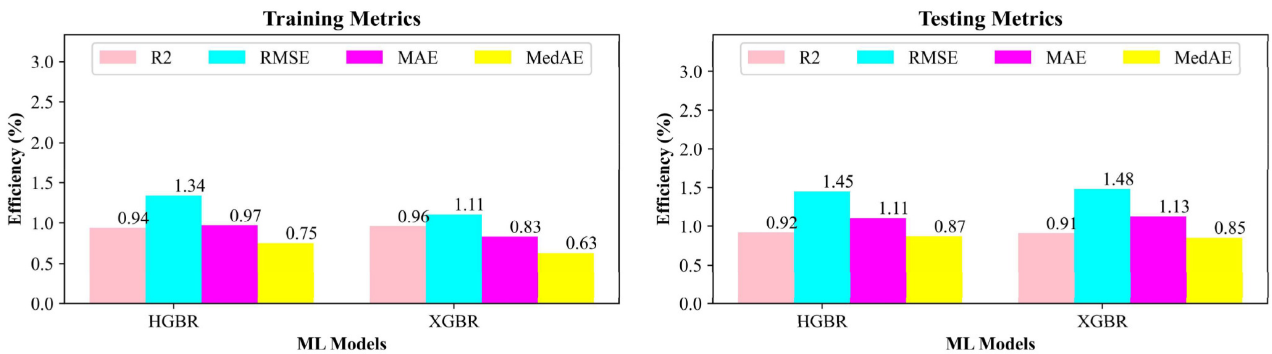

(a)

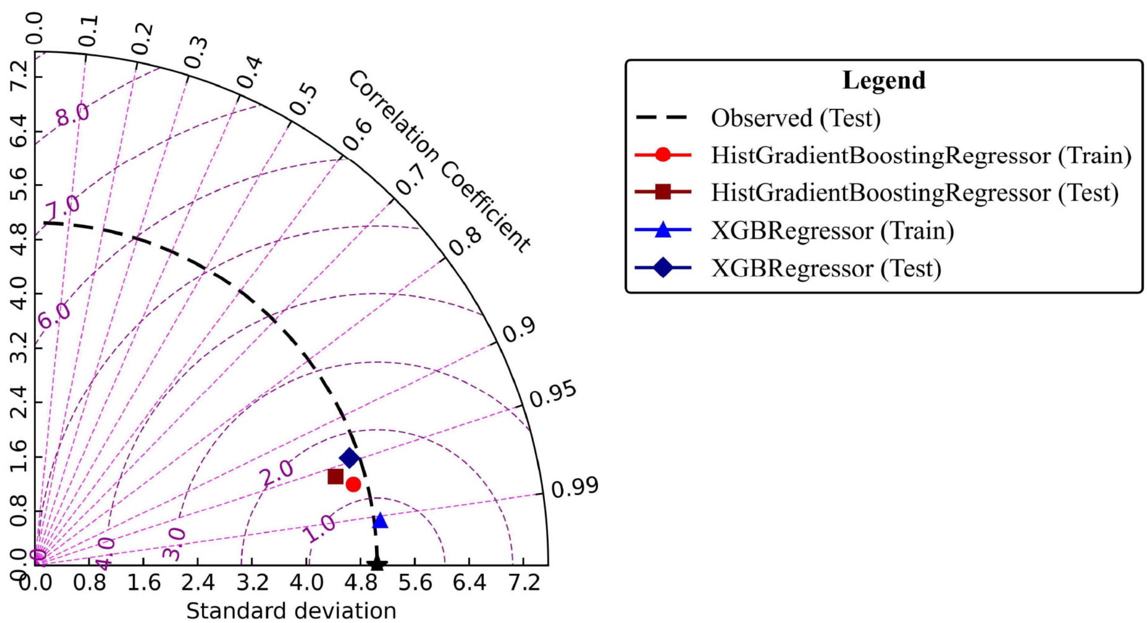

(b)

Fig. 6. Assessment of ML models by: (a) bar charts, (b) Taylor diagram.

influence of specific features on model accuracy and stability.

3.4. Lack of fit test evaluation

The lack of fit test was conducted to assess how well the HGBR and XGBR models fit the dataset by comparing the pure error and lack of fit error. For the HGBR model, the total sum of squares of errors (SSE) was 700.665 with an MSE of 1.925, and for the XGBR model, the total SSE was 565.127 with an MSE of 1.553. The pure error, calculated using predicted data from the testing phase as replicates, was 235.564 for HGBR with an MSE of 2.265 and 244.812 for XGBR with an MSE of 2.354. The lack of fit error, which is the total error minus the pure error, was 465.101 for HGBR and 320.315 for XGBR, with MSEs of 1.789 and 1.232, respectively (Table 4). The calculated F-values for HGBR and XGBR were 0.790 and 0.523, both below the critical F-value of 1.323, indicating that the lack of fit was not significant for both models. This confirms that both models passed the lack of fit test, suggesting they adequately capture the variability in the data without significant discrepancies due to the model structure itself.

4. Discussion

This study's analysis and results are positioned within the broader context of recent research in hydrological evaporation prediction, facilitating a detailed comparison with findings from other significant studies. In this study, the hybrid ML models,

Table 3. Features sensitivity analysis.

HGBR Model														
Features							Training				Testing			
Max temperature (°C)	Min temperature (°C)	Max relative humidity (%)	Sunshine (h)	Min relative humidity (%)	Rainfall (mm)	Wind speed (m/s)	R^2	RMSE	MAE	MedAE	R^2	RMSE	MAE	MedAE
							0.94	1.34	0.97	0.75	0.92	1.45	1.11	0.87
Eliminated							0.93	1.40	1.00	0.74	0.91	1.53	1.13	0.81
	Eliminated						0.94	1.34	0.98	0.74	0.91	1.54	1.19	0.88
		Eliminated					0.93	1.42	1.02	0.77	0.91	1.51	1.12	0.87
			Eliminated				0.94	1.32	0.97	0.75	0.92	1.45	1.11	0.88
				Eliminated			0.94	1.34	0.98	0.75	0.92	1.45	1.09	0.87
					Eliminated		0.93	1.35	0.98	0.80	0.90	1.60	1.21	0.93
						Eliminated	0.93	1.38	0.98	0.73	0.91	1.55	1.15	0.92
XGBR Model														
Features							Training				Testing			
Max temperature	Min temperature	Max relative humidity	Sunshine	Min relative humidity	Rainfall	Wind speed	R^2	RMSE	MAE	MedAE	R^2	RMSE	MAE	MedAE
							0.96	1.11	0.83	0.63	0.91	1.48	1.13	0.85
Eliminated							0.95	1.16	0.87	0.67	0.92	1.40	1.11	0.89
	Eliminated						0.96	1.11	0.83	0.63	0.90	1.56	1.17	0.79
		Eliminated					0.96	1.08	0.82	0.65	0.91	1.55	1.20	0.89
			Eliminated				0.96	1.11	0.83	0.62	0.91	1.47	1.13	0.79
				Eliminated			0.96	1.12	0.84	0.68	0.91	1.49	1.16	0.84
					Eliminated		0.96	1.10	0.81	0.63	0.91	1.54	1.17	0.93
						Eliminated	0.95	1.14	0.86	0.68	0.93	1.36	1.05	0.75

Table 4. Evaluation of models' lack of fit using F-statistics.

ML Models	Type of Error	Error	DF	MSE	F-value (Calculated)	F-value (Critical, alpha = 0.05)	F-test Comparison	Significance of Lack of Fit
HGBR	Total (SSE)	700.665	364	1.925	0.790	1.323	F-value (Calculated) < F-value (Critical)	Lack of Fit is not significant
	Pure (SS_{pure})	235.564	104	2.265				
	Lack of Fit (SS_{LoF})	465.101	260	1.789				
XGBR	Total (SSE)	565.127	364	1.553	0.523	1.323	F-value (Calculated) < F-value (Critical)	Lack of Fit is not significant
	Pure (SS_{pure})	244.812	104	2.354				
	Lack of Fit (SS_{LoF})	320.315	260	1.232				

particularly the integration of spectral clustering with advanced regression techniques such as HGBR and XGBR, have demonstrated substantial improvements in pan evaporation prediction. Notably, the testing phase metrics, with an R^2 of 0.92 for HGBR and 0.91 for XGBR, highlight the models' robustness. These results are competitive when compared with the findings of [44], where a deep-LSTM model for Adana station achieved an R^2 of 0.932 in similar conditions, indicating that while DL models provide slightly higher predictive accuracy, the computational efficiency and simpler implementation of regression-based models like those used in our study might offer practical advantages in certain applications. Further, [45] used GBDT model, achieving an R^2 of 0.73 indicating lower accuracy to models (i.e. HGBR and XGBR) used in our study, this could be due to the integration of spectral clustering that offers a novel approach to enhancing model performance, particularly in handling non-linear data relationships in climatic variables.

Moreover, A study [46], introduced advanced ML techniques (EEMD-MT and EEMD-SVM), which significantly improved upon traditional SVM and MT models. The findings of this study reported improvements in NSE and WI by 36 and 44.7% using EEMD-MT respectively. Similarly, in our study, the use of spectral clustering has provided a methodological advancement over traditional regression techniques, demonstrating better data segmentation and consequently, more accurate evaporation predictions. This suggests a consistent trend where hybrid and advanced methodologies tend to outperform traditional ML and empirical models in hydrological predictions. Furthermore, the improvements in RMSE and MAE in our study are consistent with those observed in [47], where TNN models were used. Both studies highlight the efficacy of advanced modeling techniques in reducing prediction errors compared to empirical models. Moreover, the application of ML to enhance prediction accuracy in pan evaporation, as seen across the studies especially [7, 8, 44–50], underscores a general consensus about the potential of these methods in environmental science.

Despite the successes reported in this paper and others, there are notable contrasts, particularly regarding the type of ML models and their specific applications. For instance, the study [44], used LSTM-GWO for forecasting evaporation shows a different approach focusing on time-series decomposition, which contrasts with our method focusing on regression enhancements through clustering. This divergence highlights the varied ways ML can be tailored to specific hydrological tasks, depending on the data characteristics and the specific requirements of the study area. Further, the comparison of results from the studies [8, 49] with our findings suggests varying degrees of effectiveness across different geographic locations and climatic conditions. While the models in [49] were specifically optimized for conditions in Iran and India, our models are more aligned with the climatic data characteristics from regions similar to those described in Paper [8], indicating that location-specific model tuning is crucial for achieving optimal performance.

In addition to aligning our results with prior research, this study adds further depth through its incorporation of interpretability and model adequacy assessments that are often overlooked. The inclusion of the Lack of Fit Test serves as a rigorous statistical validation of the models' structural soundness, ensuring that the predictive outcomes are not only statistically significant but also practically reliable. Furthermore, the use of sensitivity analysis helped uncover the specific contribution of each climatic input variable, allowing for more informed interpretation of feature importance. These components collectively enhance the confidence in the model's behavior and offer valuable guidance for future applications in diverse climatic settings.

This thorough discussion of results from this research in the context of existing literature reveals both convergences and divergences in the application and effectiveness of ML models in pan evaporation prediction. The consistently superior performance of hybrid models across most studies indicates a shift towards more complex, yet robust modeling techniques in hydrology. Meanwhile, the contrasts among different studies highlight the importance of context-specific adaptations in model development. Overall, this comparative analysis not only situates the current study within the broader research landscape but also sets a benchmark for future research, suggesting pathways for enhancing model reliability and predictive accuracy in hydrological studies.

5. Conclusion

This study addressed the pressing need for accurate pan evaporation prediction, crucial for effective water resource management in the face of changing global climate conditions. The primary objective was to enhance the prediction accuracy and reliability of pan evaporation estimates through the development of a hybrid ML model that integrates spectral clustering with advanced regression techniques. The methodology employed involved the use of spectral clustering for data preprocessing and models' performance improvements to ensure a homogeneous input for subsequent modeling with the use of two advanced regression models, HGBR and XGBR, which were rigorously tuned and validated. A sensitivity analysis was conducted to identify the impact of individual features on model performance, followed by a lack of fit test to verify the model's usability and adequacy. The results demonstrated the effectiveness of the proposed approach. Where, the HGBR model exhibited superior performance with a training R^2 of 0.94 and an RMSE of 1.34 and maintained robustness during testing with an R^2 of 0.92 and an RMSE of 1.45. Conversely, the XGBR model, while effective, showed a slight decrease in testing performance (training R^2 of 0.96 and RMSE of 1.11; testing R^2 of 0.91 and RMSE of 1.48). The closer performance metrics between training and testing phases for the HGBR model indicated a higher consistency and less susceptibility to overfitting compared to the XGBR model. In summary, this research provided three key contributions: (i) it introduced a novel use of spectral clustering to improve input data structure prior to model training. This significantly enhanced prediction accuracy; (ii) it demonstrated the practical advantage of HGBR model over XGBR model in terms of stability and generalization. It was supported by multiple statistical metrics and a lack of fit test; and (iii) it established a comprehensive evaluation framework that combined performance metrics, sensitivity analysis, and model adequacy checks. It provided a reliable blueprint for future studies in hydrological modeling. Based on these findings, it is recommended that hybrid ML models similar to the ones developed in this study be considered for broader applications in hydrological predictions. These models have shown potential for enhancing the precision and reliability of environmental forecasting tools, which are essential for planning and management in various hydrological and agricultural settings. Future research should focus on expanding the application of these models to other geographic locations to further validate their effectiveness and adaptability. Additionally, integrating more diverse climatic variables could enhance the models' predictive capabilities, catering to the specific needs of different regions affected by varying climatic impacts.

Abbreviations

ML: Machine Learning
HGBR: Histogram-based Gradient Boosting Regressor
XGBR: Extreme Gradient Boosting Regressor
LSTM: Long Short-Term Memory
NCA: Neighborhood Component Analysis
MM-ANN: Multiple model-artificial neural network
MGGP: Multi-gene Genetic Programming
DNN: Deep Neural Network
SVR: Support Vector Regression
ET: Extra Tree
XGB: Extreme Gradient Boosting
ELM: Extreme Learning Machine
WOA: Whale Optimization Algorithm
FPA: Flower Pollination Algorithm
MLP: Multilayer Perceptron
BR: Bayesian Regularization
SCG: Scaled Conjugate Gradient
GP: Gaussian Processes
ANN: Artificial Neural Network
WANN: Wavelet-based ANN
SVM-RF: Radial Function-based SVM
SVM-LF: Linear Function-based SVM
MLR: Multi-linear Regression
Cforest: Conditional Random Forest Regression
MARS: Multivariate Adaptive Regression Splines
BaggedMARS: Bagged Multivariate Adaptive Regression Splines
M5: Model Tree M5
KNN: K-nearest Neighbor
KKNN: Weighted K-nearest Neighbor
SVM: Support Vector Machine
R^2: Coefficient of Determination
RMSE: Root Mean Square Error
MAE: Mean Absolute Error
MedAE: Median Absolute Error

Conflict of interest: The authors declare no conflict of interest to any party.

References

1. C. Xu, L. Gong, T. Jiang, D. Chen, and V. P. Singh, "Analysis of spatial distribution and temporal trend of reference evapotranspiration and pan evaporation in Changjiang (Yangtze River) catchment," *J. Hydrol.*, vol. 327, no. 1–2, pp. 81–93, 2006.
2. Y. Feng, Y. Jia, Q. Zhang, D. Gong, and N. Cui, "National-scale assessment of pan evaporation models across different climatic zones of China," *J. Hydrol.*, 2018, doi: 10.1016/j.jhydrol.2018.07.013.
3. A. A. Alsumaiei, "Utility of artificial neural networks in modeling pan evaporation in hyper-arid climates," *Water*, vol. 12, no. 5, p. 1508, 2020.
4. T. A. McMahon, M. C. Peel, L. Lowe, R. Srikanthan, and T. R. McVicar, "Estimating actual, potential, reference crop and pan evaporation using standard meteorological data: A pragmatic synthesis," *Hydrol. Earth Syst. Sci.*, vol. 17, no. 4, pp. 1331–1363, 2013.
5. H. L. Penman, "Natural evaporation from open water, bare soil and grass," *Proc. R. Soc. Lond. A*, vol. 193, no. 1032, pp. 120–145, 1948.
6. M. Abed, M. A. Imteaz, and A. N. Ahmed, "A comprehensive review of artificial intelligence-based methods for predicting pan evaporation rate," *Artif. Intell. Rev.*, vol. 56, no. Suppl 2, pp. 2861–2892, 2023.
7. B. Majhi, D. Naidu, A. P. Mishra, and S. C. Satapathy, "Improved prediction of daily pan evaporation using Deep-LSTM model," *Neural Comput. Appl.*, vol. 32, no. 12, pp. 7823–7838, 2020.
8. M. Al-Mukhtar, "Modeling of pan evaporation based on the development of machine learning methods," *Theor. Appl. Climatol.*, vol. 146, no. 3, pp. 961–979, 2021.
9. L. Wang, O. Kisi, M. Zounemat-Kermani, and H. Li, "Pan evaporation modeling using six different heuristic computing methods in different climates of China," *J. Hydrol.*, vol. 544, pp. 407–427, 2017, doi: 10.1016/j.jhydrol.2016.11.059.
10. A. Malik and A. Kumar, "Pan evaporation simulation based on daily meteorological data using soft computing techniques and multiple linear regression," *Water Resour. Manag.*, vol. 29, no. 6, pp. 1859–1872, 2015, doi: 10.1007/s11269-015-0915-0.
11. G. E. Eckstein, "Water scarcity, conflict, and security in a climate change world: Challenges and opportunities for international law and policy," *Wis. Int'l LJ*, vol. 27, p. 409, 2009.
12. S. Jain, A. Srivastava, L. Khadke, U. Chatterjee, and A. Elbeltagi, "Global-scale water security and desertification management amidst climate change," *Environ. Sci. Pollut. Res.*, pp. 1–25, 2024.
13. W. Abtew, A. Melesse, W. Abtew, and A. Melesse, "Evaporation and evapotranspiration estimation methods," *Evaporation Evapotranspiration Meas. Estim.*, pp. 63–91, 2013.
14. J. D. Owusu-Sekyere, E. A. Ampofo, and O. Asamoah, "Comparison of five different methods in estimating reference evapotranspiration in Cape Coast, Ghana," 2017.
15. C. Che and J. Tian, "Understanding the interrelation between temperature and meteorological factors: A case study of szeged using machine learning techniques," *J. Comput. Technol. Appl. Math.*, vol. 1, no. 4, pp. 47–52, 2024.
16. Z. H. Doost *et al.*, "Development of intensity–duration–frequency curves for Herat, Afghanistan: Enhancing flood risk management and implications for infrastructure and safety," *Nat. Hazards*, 2024, doi: 10.1007/s11069-024-06730-x.
17. L. Wang, O. Kisi, B. Hu, M. Bilal, M. Zounemat-Kermani, and H. Li, "Evaporation modelling using different machine learning techniques," *Int. J. Climatol.*, vol. 37, no. S1, pp. 1076–1092, 2017.
18. W. J. M. Lakmini Prarthana Jayasinghe, R. C. Deo, A. Ghahramani, S. Ghimire, and N. Raj, "Development and evaluation of hybrid deep learning long short-term memory network model for pan evaporation estimation trained with satellite and ground-based data," *J. Hydrol.*, vol. 607, no. April 2021, p. 127534, 2022, doi: 10.1016/j.jhydrol.2022.127534.
19. A. Malik *et al.*, "Modeling monthly pan evaporation process over the Indian central Himalayas: Application of multiple learning artificial intelligence model," *Eng. Appl. Comput. Fluid Mech.*, vol. 14, no. 1, pp. 323–338, 2020.
20. A. El Bilali, T. Abdeslam, N. Ayoub, H. Lamane, M. A. Ezzaouini, and A. Elbeltagi, "An interpretable machine learning approach based on DNN, SVR, Extra Tree, and XGBoost models for predicting daily pan evaporation," *J. Environ. Manage.*, vol. 327, p. 116890, 2023.
21. L. Wu, G. Huang, J. Fan, X. Ma, H. Zhou, and W. Zeng, "Hybrid extreme learning machine with meta-heuristic algorithms for monthly pan evaporation prediction," *Comput. Electron. Agric.*, vol. 168, p. 105115, 2020, doi: 10.1016/j.compag.2019.105115.
22. P. Aghelpour, Z. Bagheri-Khalili, V. Varshavian, and B. Mohammadi, "Evaluating three supervised machine learning algorithms (LM, BR, and SCG) for daily pan evaporation estimation in a semi-arid region," *Water (Switzerland)*, vol. 14, no. 21, pp. 1–23, 2022, doi: 10.3390/w14213435.
23. A. A. Alsumaiei, "Modeling high pan evaporation losses using support vector machine, Gaussian processes, and regression tree models," *J. Hydrol. Eng.*, vol. 29, no. 5, p. 4024029, 2024.
24. M. Kumar *et al.*, "The superiority of data-driven techniques for estimation of daily pan evaporation," *Atmosphere (Basel)*, vol. 12, no. 6, p. 701, 2021.
25. K. Khosravi *et al.*, "Enhancing pan evaporation predictions: Accuracy and uncertainty in hybrid machine learning models," *Ecol. Inform.*, vol. 85, p. 102933, 2025.
26. N. J. Rasheed, M. S. Al-Khafaji, I. A. Alwan, M. S. Al-Suwaiyan, Z. H. Doost, and Z. M. Yaseen, "Survey on the resolution and accuracy of input data validity for SWAT-based hydrological models," *Heliyon*, vol. 10, no. 19, 2024.
27. J. Liu and J. Han, "Spectral clustering," in *Data clustering*, Chapman and Hall/CRC, 2018, pp. 177–200.
28. U. Von Luxburg, "A tutorial on spectral clustering," *Stat. Comput.*, vol. 17, pp. 395–416, 2007.
29. D. Niu, J. Dy, and M. I. Jordan, "Dimensionality reduction for spectral clustering," in *Proceedings of the Fourteenth International Conference on Artificial Intelligence and Statistics*, 2011, pp. 552–560.
30. F. R. Bach and M. I. Jordan, "Learning spectral clustering, with application to speech separation," *J. Mach. Learn. Res.*, vol. 7, pp. 1963–2001, 2006.
31. W. Chen and G. Feng, "Spectral clustering: A semi-supervised approach," *Neurocomputing*, vol. 77, no. 1, pp. 229–242, 2012.
32. O. A. Alawi *et al.*, "Development of optimized machine learning models for predicting flat plate solar collectors thermal efficiency associated with Al2O3-water nanofluids," *Eng. Appl. Artif. Intell.*, vol. 133, p. 108158, 2024.
33. A. Guryanov, "Histogram-based algorithm for building gradient boosting ensembles of piecewise linear decision trees," 2019. doi: 10.1007/978-3-030-37334-4_4.
34. T. Kishida, R. W. Boulanger, N. A. Abrahamson, T. M. Wehling, and M. W. Driller, "Regression models for dynamic properties of highly organic soils," *J. Geotech. geoenvironmental Eng.*, vol. 135, no. 4, pp. 533–543, 2009.
35. D. A. Tran *et al.*, "Evaluating the predictive power of different machine learning algorithms for groundwater salinity

prediction of multi-layer coastal aquifers in the Mekong Delta, Vietnam," *Ecol. Indic.*, vol. 127, p. 107790, 2021.
36. R. Piraei, M. Niazkar, S. H. Afzali, and A. Menapace, "Application of machine learning models to bridge afflux estimation," *Water*, vol. 15, no. 12, p. 2187, 2023.
37. J. Ge *et al.*, "Prediction of greenhouse tomato crop evapotranspiration using XGBoost machine learning model," *Plants*, vol. 11, no. 15, p. 1923, 2022.
38. T. Chen and C. Guestrin, "Xgboost: A scalable tree boosting system," in *Proceedings of the 22nd acm sigkdd international conference on knowledge discovery and data mining*, 2016, pp. 785–794.
39. Z. H. Doost, L. Goliatt, M. S. Aldlemy, M. Ali, and B. da S. Macêdo, "Enhancing predictive accuracy of compressive strength in recycled concrete using advanced machine learning techniques with K-means clustering," *AUIQ Tech. Eng. Sci.*, vol. 1, no. 1, p. 10, 2024.
40. D. Chicco, M. J. Warrens, and G. Jurman, "The coefficient of determination R-squared is more informative than SMAPE, MAE, MAPE, MSE and RMSE in regression analysis evaluation," *Peerj Comput. Sci.*, vol. 7, p. e623, 2021.
41. A. Colin Cameron, F. A. G. Windmeijer, C. A. Colin, Frank A. G Windmeijer, A. Colin Cameron, and F. A. G. Windmeijer, "An R-squared measure of goodness of fit for some common nonlinear regression models," *J. Econom.*, vol. 77, no. 2, pp. 329–342, Apr. 1997, doi: 10.1016/S0304-4076(96)01818-0.
42. T. O. Hodson, "Root mean square error (RMSE) or mean absolute error (MAE): When to use them or not," *Geosci. Model Dev. Discuss.*, vol. 2022, pp. 1–10, 2022.
43. J.-M. Sánchez-González, C. Rocha-de-Lossada, and D. Flikier, "Median absolute error and interquartile range as criteria of success against the percentage of eyes within a refractive target in IOL surgery," *J. Cataract Refract. Surg.*, vol. 46, no. 10, p. 1441, 2020.
44. O. Kisi, A. Mirboluki, S. R. Naganna, A. Malik, A. Kuriqi, and M. Mehraein, "Comparative evaluation of deep learning and machine learning in modelling pan evaporation using limited inputs," *Hydrol. Sci. J.*, no. just-accepted, 2022.
45. X. Lu, Y. Ju, L. Wu, J. Fan, F. Zhang, and Z. Li, "Daily pan evaporation modeling from local and cross-station data using three tree-based machine learning models," *J. Hydrol.*, vol. 566, no. July, pp. 668–684, 2018, doi: 10.1016/j.jhydrol.2018.09.055.
46. M. Rezaie-Balf, O. Kisi, and L. H. C. Chua, "Application of ensemble empirical mode decomposition based on machine learning methodologies in forecasting monthly pan evaporation," *Hydrol. Res.*, vol. 50, no. 2, pp. 498–516, Apr. 2019, doi: 10.2166/nh.2018.050.
47. M. Abed, M. A. Imteaz, and A. N. Ahmed, "Utilising machine learning for pan evaporation prediction-A case study in western Australia," *Iaeng. org*, 2023.
48. M. Abed, M. A. Imteaz, A. N. Ahmed, and Y. F. Huang, "Modelling monthly pan evaporation utilising random forest and deep learning algorithms," *Sci. Rep.*, vol. 12, no. 1, p. 13132, 2022, doi: 10.1038/s41598-022-17263-3.
49. A. Malik *et al.*, "Deep learning versus gradient boosting machine for pan evaporation prediction," *Eng. Appl. Comput. Fluid Mech.*, vol. 16, no. 1, pp. 570–587, 2022.
50. H. Wang, F. Sun, F. Liu, T. Wang, W. Liu, and Y. Feng, "Reconstruction of the pan evaporation based on meteorological factors with machine learning method over China," *Agric. Water Manag.*, 2023, doi: 10.1016/j.agwat.2023.108416.